Journal of Applied Physics

RESEARCH ARTICLE | APRIL 10 2023

Effect of a niobium-doped PZT interfacial layer thickness on the properties of epitaxial PMN-PT thin films

M. Boota ; E. P. Houwman ; G. Lanzara ; G. Rijnders

Journal of Applied Physics 133, 145302 (2023)
https://doi.org/10.1063/5.0139426

Journal of Applied Physics ARTICLE scitation.org/journal/jap

Effect of a niobium-doped PZT interfacial layer thickness on the properties of epitaxial PMN-PT thin films

Cite as: J. Appl. Phys. **133**, 145302 (2023); doi: 10.1063/5.0139426
Submitted: 20 December 2022 · Accepted: 21 March 2023 ·
Published Online: 10 April 2023

M. Boota,[1,2,a)] E. P. Houwman,[1,b)] G. Lanzara,[2] and G. Rijnders[1]

AFFILIATIONS

[1]MESA+ Institute for Nanotechnology, University of Twente, P.O. Box 217, 7500AE Enschede, The Netherlands
[2]Engineering Department, University of Rome "ROMA TRE," Via Della Vasca Navale 79, 00146 Rome, Italy

[a)]**Current address:** Department of Physics, The University of Lahore, 1-km Defense Road, Lahore, Pakistan.
[b)]**Author to whom correspondence should be addressed:** e.p.houwman@utwente.nl

ABSTRACT

We are reporting on high quality epitaxial thin films of $[Pb(Mg_{1/3}Nb_{2/3})O_3]_{0.67}$-$(PbTiO_3)_{0.33}$ [PMN-PT (67/33)]. These films were deposited on (001) oriented, vicinal $SrTiO_3$ single crystal substrates, using 1 mol. % niobium-doped $Pb(Zr_{0.52},Ti_{0.48})O_3$ (Nb-PZT) as an interfacial layer. The functional properties of the epitaxial PMN-PT (67/33) thin films were investigated as a function of the layer thickness of the Nb-PZT layer. The deposited hetero-structures are perovskite phase pure and fully (001)-oriented. The variation in Nb-PZT interfacial layer thickness results in an increasing trend change of the in-plane lattice parameter of that layer, which in turn causes a decrease in the c/a ratio of the PMN-PT film on top. The most noticeable effect related to this is a decrease in built-in-bias (imprint) voltage. Thus, the built-in bias can be tuned by changing the interfacial layer thickness. The ferroelectric capacitor properties are found to be most stable for the thinnest interfacial layers under a high number (10^8) of switching cycles.

I. INTRODUCTION

Lead based piezo-ceramics are much investigated materials for use in devices for energy conversion from mechanical energy into electrical energy and vice versa, for example, in transducer, sensor, and actuator applications.[1] $[Pb(Mg_{1/3}Nb_{2/3})O_3]_{0.67}$-$(PbTiO_3)_{0.33}$ (PMN-PT) is a very interesting material because it can exhibit high strain under an applied electrical field. PMN-PT, in single crystalline form, is one of the ferroelectric materials with the strongest piezoelectric responses, which makes it a material of first choice for hyperactive piezo-MEMS devices. PMN-PT in its bulk crystalline form exhibits an outstanding electromechanical coupling coefficient and a large dielectric constant with weak temperature dependence around room temperature. The latter feature makes PMN-PT and also other lead based relaxor ferroelectrics interesting for numerous applications.[2] Single crystals of PMN-PT show one order of magnitude higher piezoelectric response compared to the most prominent and investigated lead zirconate titanate bulk piezo-ceramics, $PbZr_{0.52}Ti_{0.48}O_3$ (PZT).[3,4]

Deposition of perovskite phase pure deposition of PMN-PT films is a pre-requisite to obtain good properties. The desired phase pure growth is known to be difficult because of its relatively poor thermodynamic stability as compared to the undesired pyrochlore phases. The main processing difficulty associated with the growth of the pure perovskite phase is the control over the PMN-PT stoichiometry in this system due to lead (Pb) losses during the growth process.[5–8] The commonly used approach employing thin film growth technology is the careful adjustment of the processing parameters during the growth process. The deposition parameters are typically adjusted to minimize the evaporation of the lead (Pb) at high deposition temperature.[9] The second approach involves the substrates on which the thin films are deposited. The use of a high miscut substrate is reported to be beneficial for retaining the right stoichiometry of the PMN-PT thin films on vicinal cut single crystal $SrTiO_3$ as well as on silicon substrates.[4,10] The miscut substrates provide more binding sites for the volatile element (Pb) during growth, thus suppressing the Pb loss and resulting in

stoichiometric films. The third approach involves the use of additional interlayers and their roughness to improve the incorporation of the volatile element (Pb). The roughness of the $LaNiO_3$ bottom electrode interfacial layer has also been reported to promote the phase pure growth of the PMN-PT thin films. The interfacial roughness is helpful to increase the incorporation of the volatile element (Pb), hence promoting the phase pure growth of the deposited films of the PMN-PT.[11] The use of lead based epitaxial PZT thin films between the bottom electrode and PMN-PT was shown to be beneficial for stabilization of the right PMN-PT phase. The lead (Pb) based perovskite interfacial layer enhances the bonding sites of the volatile element (Pb), hence promoting the subsequent phase pure growth of PMN-PT.[12] Thus, perovskite phase pure epitaxial PMN-PT films can be grown, using deposition techniques such as pulsed laser deposition (PLD), magnetron sputtering (RF), or chemical vapor deposition (CVD).[13–19]

Previously, we have reported on the growth of epitaxial thin films of PMN-PT, employing a 25 nm thick hard (Fe), soft (Nb), or an un-doped epitaxial PZT layer sandwiched between the PMN-PT and the $SrRuO_3$ bottom electrode. PMN-PT films with 1 mol. % Nb-doped $Pb(Zr_{0.52}Ti_{0.48})O_3$ were shown to exhibit a higher self-bias voltage as compared to the other hetero-structures.[19] In this study, we report the results of similar epitaxial PMN-PT films grown on 1 mol. % Nb-doped PZT layers with varying thickness, in the range 13–100 nm. The effect of the Nb-PZT layer thickness on the ferroelectric, dielectric, self-bias voltage, and crystalline properties of epitaxial PMN-PT films is investigated.

II. MATERIALS AND METHODS

In this study, 0.5 mm thick single crystal (001) oriented, miscut (0.4^0) $SrTiO_3$ (STO) was selected as a substrate for its well defined crystalline surface. To achieve B-site (TiO_2) surface termination of the substrates, a procedure developed by Koster and co-workers was used.[20] The B-site (TiO_2) surface termination of the STO substrates was necessary to obtain a uniform and high quality thin film of a 100 nm thick layer of $SrRuO_3$ (SRO) that was used as a bottom electrode.[21] SRO was also used as a top electrode. The $[Pb(Mg_{1/3}Nb_{2/3})O_3]_{0.67}$-$(PbTiO_3)_{0.33}$ (PMN-PT) composition was chosen for its giant piezo-response in the thin film form reported in the literature.[4] The 1 mol. % Nb-doped $Pb(Zr_{0.52}Ti_{0.48})O_3$ (Nb-PZT) composition was selected, because of the earlier found high self-bias field.[19]

The complete hetero-structures (STO/SRO/Nb-PZT/PMN-PT/SRO) were deposited by pulsed laser deposition (PLD). The PLD system is equipped with a KrF excimer laser with an ~25 ns pulse and operates at 248 nm wavelength. Before deposition, the vacuum chamber was pumped down to a base pressure below 1×10^{-7} mbar and the substrate was heated to 600 °C (deposition temperature of the SRO bottom electrode). The thickness of the SRO bottom and top electrodes was fixed at 100 nm. The thickness of the Nb-PZT interfacial thin layer was varied and has nominal thicknesses of 13, 25, 50, and 100 nm, respectively (relative ratio 1:2:4:8). The layer thicknesses were calculated from the deposition rate of an approximately 500 nm thick film, which thickness was determined from cross sectional SEM imaging and that was deposited from the same target in the same deposition system, using the same deposition conditions, as were used for the Nb-PZT films in this study. The PMN-PT layer thickness was fixed at approximately 200 nm for all samples. The complete layer stack was deposited without breaking the vacuum. Immediately after the deposition of the layer stack, the hetero-structures were cooled down to room temperature in oxygen ambient at a cooling rate of 10 °C min^{-1}. Further details on the deposition conditions of the SRO, Nb-PZT, and PMN-PT are reported elsewhere.[19]

The crystal structure and epitaxial relations of the deposited layer stacks were investigated by x-ray diffraction. A HR-XRD (PANalytical X1 pert PRO MRD) with Cu-Kα1 radiation (λ = 1.5406 Å) was used to record θ-2θ diffractograms, ω-scans (rocking curves), and reciprocal space maps. From the reciprocal space maps, the lattice parameters were determined. To perform the electrical measurements, the layer stack was patterned into capacitor structures with parallel plate geometry ($200 \times 200\,\mu m^2$) using standard optical photolithography processes. These patterns were structured by argon ion beam etching. To investigate the ferroelectric properties of the devices, polarization vs electric field measurements (P–E hysteresis loops) were recorded with a modified Sawyer Tower circuit (AixACCT TF Analyser 3000). The P–E loops were recorded by applying a 1 kHz, bipolar, triangular pulse with an amplitude of 150 kV cm^{-1}. Ferroelectric response stability (fatigue) was investigated with a 150 kV cm^{-1} bipolar, rectangular pulse train of 10 kHz (frequency). A laser Doppler vibrometer (Polytec MSA-400) was employed to determine the piezoelectric response of the devices, by recording the electric field vs d_{33} loops. The electric field vs capacitance (E-C) curves of the ferroelectric capacitors were recorded with a 10 kHz small amplitude AC signal over a range of ±150 kV/cm AC-excitation signal, using a Keithley 4200 and Suss MicroTech PM300 probe station. The dielectric constants were calculated from these curves.

III. RESULTS AND DISCUSSIONS

A. Structural properties

The diffraction patterns (θ–2θ scans) of the epitaxial thin films of PMN-PT with a Nb-PZT interfacial layer with varying thickness are shown in Fig. 1(a). The positions of the diffraction peaks due to the substrate, SRO bottom electrode, PMN-PT, and the Nb-PZT interfacial layer are indicated in Fig. 1(b) by the dashed black lines. The positions of the peaks corresponding to bulk material lattice parameters are indicated by the solid green lines. All reflection peaks correspond to (001) growth of the layers and no reflections corresponding to pyrochlore phases or other growth orientations were detected. This demonstrates that the deposited films are perovskite, phase pure and (001) oriented within the detection limits of our instrument.

The diffraction peaks of the Nb-PZT interfacial layers are slightly shifted from the unstrained Nb-PZT value. This suggests that these layers are in-plane compressively strained, giving rise to a small expansion of the unit cell in the out-of-plane direction. This is expected because of the compressive strain imposed by the STO substrate. A broad shoulder on the Nb-PZT reflection toward the lower angle side is observed for all Nb-PZT layer thicknesses, indicating the presence of a strain gradient in the interfacial layer. Strain relaxation with increasing film thickness is typically observed in (thin) epitaxial PZT films on STO.[12] The formation of structural

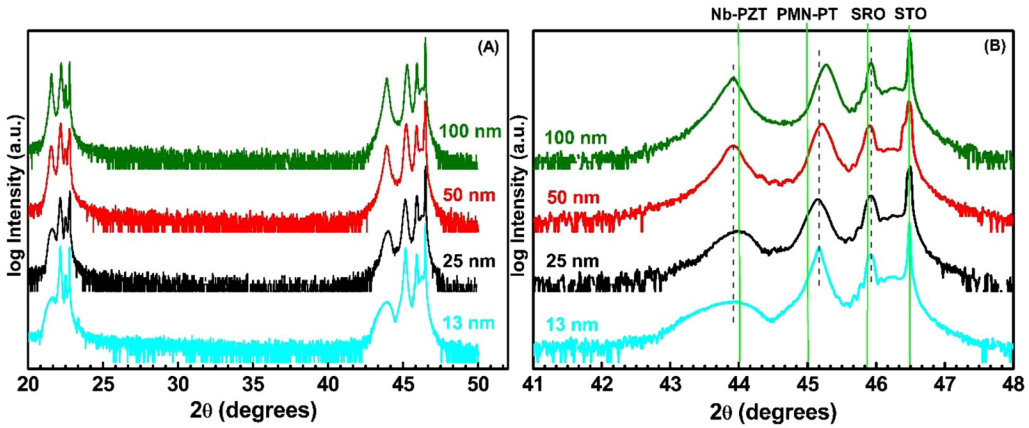

FIG. 1. XRD patterns of 200 nm thick PMN-PT films deposited on Nb-PZT interfacial layer with four different thicknesses on 100 nm SRO and STO (001) substrates (a). Zoom-in of the (002) diffraction peaks area indicating peak shift (change in out of plane lattice constants) due to varying interfacial layer thickness. The bulk peak positions are marked with solid green lines, while dotted lines are drawn to highlight peak shifts (b).

defects like misfit dislocations is generally believed to be the reason for the strain relaxation.[22] The strain gradient layer thickness is of the order of the thinnest layer, i.e., in the range 10–20 nm, since for larger Nb-PZT layer thicknesses, the shoulder does not change anymore.

The reflections corresponding to the PMN-PT layers are shifted away from the bulk angle for unstrained, rhombohedral PMN-PT, indicating a decrease in the out of plane lattice parameter of the PMN-PT layers with increasing interfacial layer thickness. The PMN-PT film (pseudocubic $a_{bulk} \approx 4.02$ Å) deposited on top of the Nb-PZT interfacial layer (tetragonal $a_{bulk} \approx 4.05$ Å, $c_{bulk} \approx 4.11$ Å) is under in-plane tensile strain.[4]

Figure 2(a) shows the (in-plane and out-of-plane) lattice parameters of the Nb-PZT and PMN-PT layers as a function of the Nb-PZT interfacial layer thickness. These were obtained from reciprocal space maps (RSMs, not shown here). The values are also given in Table S1 in the supplementary material. It is seen that the average lattice parameters of the Nb-PZT layer have relaxed to approximately the bulk Nb-PZT values after 30–50 nm. (As these are average lattice parameters for these thicknesses this means that the local lattice parameters already must have relaxed to the bulk values at smaller Nb-PZT thickness values.) The c/a ratio of the Nb-PZT also relaxes to the bulk value [Fig. 2(b)] as does the unit cell volume V_{uc} [Fig. 2(c)]. The strongly tetragonally deformed Nb-PZT unit cell for the thinnest layers has a lower unit cell volume, indicating the presence of a significant density of lattice defects. In general, it is thought that V_{uc} increases due to the presence of oxygen vacancies, hence the observed *reduction* in V_{uc} might suggest that other defect types are the dominating cause of the strain relaxation. It is also seen that the PMN-PT film is under tensile in-plane strain that increases very slightly and linearly with the Nb-PZT layer thickness. The c/a ratio of PMN-PT decreases from a value nearly equal to 1 to a substantially reduced value of 0.992 with increasing in-plane lattice mismatch of the PMN-PT and the Nb-PZT. The V_{uc} of PMN-PT is within the error margins equal to the bulk value and nearly independent of the Nb-PZT

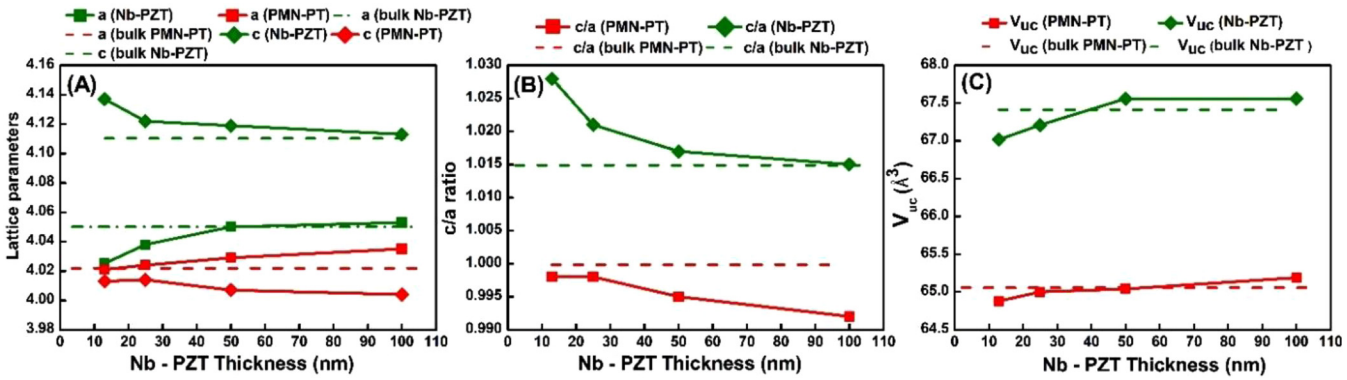

FIG. 2. (a) Lattice parameters of Nb-PZT and PMN-PT. (b) c/a ratio of Nb-PZT and PMN-PT. (c) Unit cell volume of Nb-PZT and PMN-PT.

layer thickness and the imposed strain (although a weak increasing trend might be observed). This suggests that PMN-PT can be elastically deformed in this strain range without the introduction of strain relaxation defects.

Rocking curve measurements (Fig. S3 in the supplementary material) on PMN-PT films show a full width at half maximum (FWHM) in the range 0.4°–0.11° for the (002) ω-scans. Commercially available bulk single crystals of PMN-PT have an FWHM of 0.14° for the same reflection.[4] The comparable values for the thin films demonstrate the excellent degree of oriented growth as well as superb crystalline quality of our PMN-PT thin films. Rocking curve measurements also exhibit excellent sample to sample reproducibility and thus crystalline quality of the deposited hetero-structures in this study.

B. Ferroelectric, dielectric, and piezoelectric properties

Polarization (P–E) hysteresis loops, relative dielectric constant curves obtained from the electric field vs capacitance curves, and d_{33} hysteresis loops recorded for the Nb-PZT/PMN-PT capacitor devices are shown in Fig. 3.

The ferroelectric hysteresis loops are significantly different for the four different Nb-PZT layer thicknesses: the *maximum polarization* reached at 150 kV/cm is largest for the stacks with the thinnest Nb-PZT layer; for the same devices, there is a significant shift of the loops in the negative field direction, indicating the presence of a built-in field; the loops of the devices with thicker Nb-PZT are more slanted and consequently show lower remanent polarization values; the same devices have slightly larger coercive field values. For all devices, the high-field slope of the loops is approximately the same, implying that the average high-field polarization responses are very similar.

The *total polarization* of the device arises from the thickness weighted sum of the polarizations in the Nb-PZT and PMN-PT layer. The polarization contribution from the Nb-PZT layer scales as $t_{Nb-PZT}/(t_{Nb-PZT} + t_{PMN-PT})$, thus varies from $13/213 \approx 0.06$ to $100/300 \approx 0.33$. The average length of the out-of-plane component of the Nb-PZT polarization vector is expected to decrease slightly because the average compressive strain in the Nb-PZT decreases, reducing the tetragonality of the unit cell. Further, the average tensile strain in the PMN-PT increases with Nb-PZT layer thickness. This causes the PMN-PT polarization vector to rotate into plane, reducing the measured out-of-plane component in the PMN-PT. This can explain the overall reduction in polarization with increasing Nb-PZT thickness. For the smallest Nb-PZT thickness, we observe less polarization than for the 25 nm device. Apparently, in this case, the polarization increase arising from the Nb-PZT fraction is apparently larger than the decrease due to polarization rotation in the PMN-PT.

The *loop shifts*, observed in the polarization, as well as in the capacitance and piezoelectric constant measurements, indicate the presence of a self-bias field which is much more negative for the thin Nb-PZT interfacial layers than for the thick layers. The built-in bias is likely to be caused by the combined effect of the charged Nb-PZT layer and the strain gradient in this layer. The strain gradient layer contributes to the built-in electrical field through the flexo-electric effect, next to the effect of the charge in the Nb-doped layer.[12] The latter effect is thought to be due to the presence of a non-switchable, but polarized, dielectric layer at the electrode–Nb-PZT interface. It is not straightforward to disentangle the combined effect of these two mechanisms.

It is noted that the *self-bias field* has several important consequences, which may be of benefit in certain applications. First, due to the loop shift, the magnitude of, in this case, positive remanent polarization (P_r) will be enhanced and is increasing with a higher self-bias field (see Table S2 in the supplementary material). Second, the polarization in a certain preferential direction will be stabilized as a consequence of self-bias field. The imprint will stabilize the polarization in the downward direction for the films reported in this study. Consequently, piezoelectric devices fabricated using these films are expected to exhibit less fatigue in unipolar operation as, for example, in piezo-response devices.[22,23] This will mitigate the commonly reported low coercive field of doped single crystals of PMN-PT.

Slanting of the polarization loop in general can be ascribed to the presence of a dielectric layer,[24] which in the present devices may be due to the strain gradient layer and probably is the main cause of the slanting in the 13 and 25 nm devices. A second cause for slanting can be a distribution in switching fields in the ferroelectric layer stack, which we think is largely determined by the

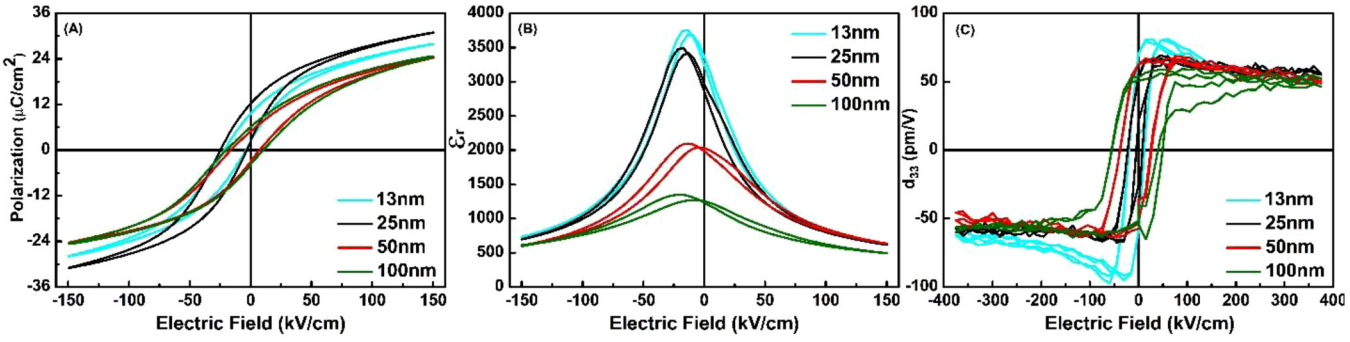

FIG. 3. Electric field vs polarization hysteresis loops of PMN-PT films deposited on top of four different thicknesses of Nb-PZT interfacial layer (a), relative dielectric constant vs electric field curves (b), and d_{33} loops (c).

Nb-PZT layer. The increased slanting of the loops with increasing Nb-PZT thickness is then attributed to the increasing fraction of the Nb-PZT layer with a larger spread in coercive fields.

The coercive fields are slightly increased for the thicker ferroelectric Nb-PZT interfacial layers but are still substantially smaller than found for most PZT capacitors. For an ideal relaxor, the coercive field is very small; however, here we see that the presence of the ferroelectric interfacial layer causes finite coercive field values.

The large slopes and remanent polarization values of the P–E loops of the capacitors with thin Nb-PZT sandwiched layers are reflected in the high peaks in the relative dielectric constant curves of these devices. The self-bias field causes a shift of the permittivity curves in the negative field direction. This has an important consequence when these films are used in piezoelectric sensing or energy-harvesting devices. It reduces the relative dielectric constant at zero field (see Table S2 in the supplementary material) and thus enhances the figure of merit ($FOM = e_{31}^2/\varepsilon_0\varepsilon_r$). Nagarajan and co-workers investigated the effects of strain on the dielectric constants of epitaxial thin films of PMN-PT (90/10) and observed an increase in the zero-field dielectric constant with strain relaxation in the PMN-PT,[25] as we see here as well for decreasing Nb-PZT thickness.

The d_{33} hysteresis loops are similar in terms of maximum piezoelectric response and bias field dependence, apart from the loop for 13 nm Nb-PZT, which shows a significantly larger maximum d_{33} value and significant field dependence. We ascribe this to the dominant PMN-PT volume fraction in this device.

The ferroelectric, dielectric, and piezoelectric properties of the hetero-structures reported in this study are summarized in Table S2 in the supplementary material.

C. Stability of the ferroelectric response

The stability of the ferroelectric response (aging behavior) of the ferroelectric capacitor devices with different Nb-PZT thicknesses was investigated by subjecting the devices to a large number (10^8) of bipolar switching cycles. The remnant polarization, self-bias field $[E_{sb} = (E_c^+ + E_c^-)/2]$, and average coercive field $[E_{c,av} = (E_c^+ - E_c^-)/2]$ are shown in Fig. 4 as a function of the number of fatigue cycles.

The ferroelectric capacitor devices with the 13 nm Nb-PZT layer show an excellent stability. Hardly any change in remnant polarization, coercive field, and built-in-bias field is observed. However, with increasing Nb-PZT thickness, ferroelectric response changes upon cycling and is significant for the device with the largest Nb-PZT thickness. The change sets in above about 3×10^6 cycles. The coercive field increases significantly, indicating an increase in the pinning of the domain walls. We attribute this to a change in the defect charge distribution in the Nb-PZT layer under

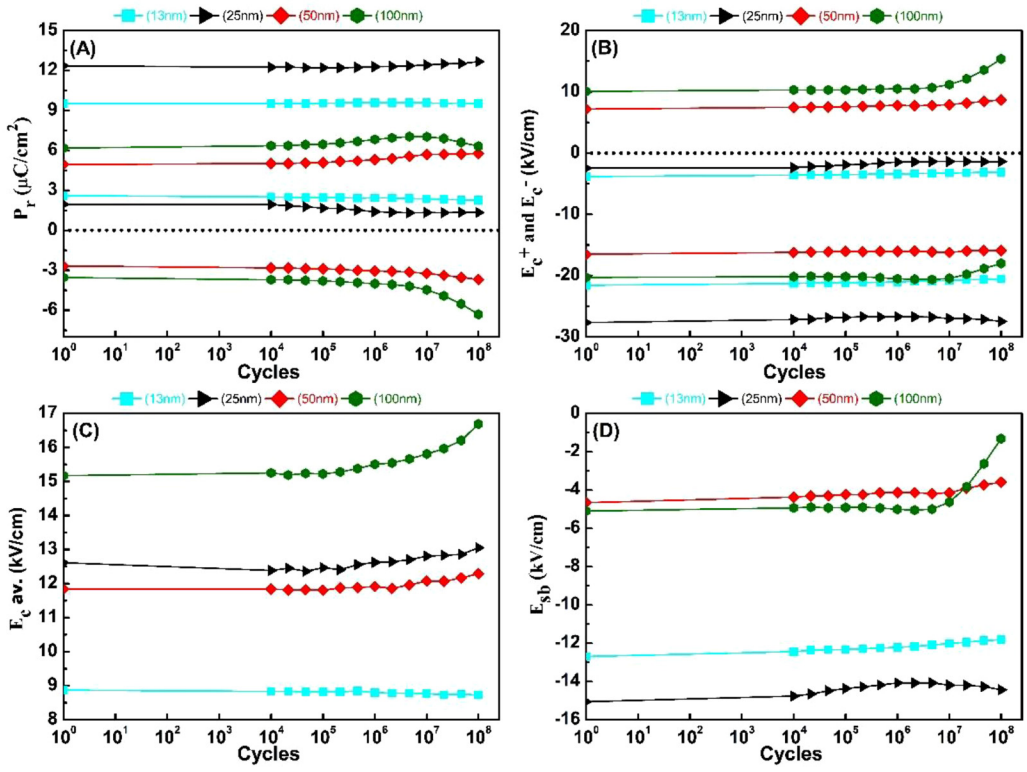

FIG. 4. Remnant polarization vs number of cycles performance of epitaxial PMN-PT films deposited using different thicknesses of Nb-PZT interfacial layer (a), coercive field vs number of cycles performance (b), $E_{c,av}$ vs number of cycles (c), and self-bias vs number of cycles (d).

the field cycling. The increased mobility of the defect charges is likely related to the more relaxed strain state of the major part in this film. We expect that the change in self-bias field is related to the same effect. With increasing coercive field, one also expects an increase in remanent polarization in slanted loops, as is also observed. This analysis shows that PMN-PT films deposited on top of a thin interfacial layer show better stability of the ferroelectric response than films deposited on thicker interfacial layers.

Finally, we need to address the role of the Nb doping of the interfacial layer. One expects that a strain free Nb-PZT layer contains relatively many oxygen vacancies that are needed to compensate the 5+ charges of the Nb-ions and keep the Nb-PZT layer charge neutral. We think that the consequence of the large defect density is that the layer is more compliant toward deformations (lower Young's modulus). This is supported by the observation that the average lattice parameters of the Nb-PZT layer can absorb large deformations over substantial layer thicknesses. For the 13 nm layer, the c/a is increased from the bulk value of 1.015 to 1.028. Even for 26 nm, the deformation is still large. [Note that the c/a ratio in the first Nb-PZT monolayer, growing epitaxially strained to the SRO (which has the same in-plane lattice parameter as the underlying STO substrate), and assuming no strain relaxation in this layer by defects or additional lattice vacancies is as large as 1.13.]

IV. CONCLUSIONS

High crystalline quality, perovskite phase pure and (001) oriented, epitaxial PMN-PT films were deposited on a Nb-PZT interfacial layer with varying thicknesses. These hetero-structures show a strain variation in both ferroelectric layers (PMN-PT, Nb-PZT). The strain variations in the ferroelectric layers cause a noticeable effect on the properties of the ferroelectric capacitors. The strain in the ferroelectric layers causes the development of the self-bias field in the hetero-structure. The built-in bias can be tuned by changing the interfacial layer thickness. The built-in bias might be beneficial for devices that operate at zero bias voltage like energy scavengers and low energy consumption sensors.[26]

SUPPLEMENTARY MATERIAL

In the supplementary material, the data given in Figs. 2 and 4 are provided in numerical form in Tables S1 and S2, respectively. The self-bias fields, remanent field, and piezoelectric coefficient values at low cycle number are compared in Fig. S1.

ACKNOWLEDGMENTS

The research work reported in this paper has been financially supported by the Engineering Doctorate School of Universita Degli Studi Roma Tre and by NanoNextNL, a micro- and nanotechnology consortium of the Government of the Netherlands and 130 partners.

AUTHOR DECLARATIONS

Conflict of Interest

The authors have no conflicts to disclose.

Author Contributions

M. Boota: Formal analysis (lead); Investigation (lead); Writing – original draft (lead). **E. P. Houwman:** Formal analysis (equal); Investigation (supporting); Supervision (lead); Writing – original draft (equal); Writing – review & editing (equal). **G. Lanzara:** Supervision (supporting). **G. Rijnders:** Resources (lead); Supervision (supporting); Writing – review & editing (supporting).

DATA AVAILABILITY

The data that support the findings of this study are available within the article and its supplementary material.

REFERENCES

[1]H. S. Tzou and C. I. Tseng, J. Sound Vib. **138**, 17 (1990).
[2]Z. Kutnjak, J. Petzelt, and R. Blinc, Nature **441**, 956 (2006).
[3]S. E. Park and T. R. Shrout, J. Appl. Phys. **82**, 1804 (1997).
[4]S. H. Baek, J. Park, D. M. Kim *et al.*, Science **334**, 958, (2011).
[5]D. Lavric, R. A. Rao, Q. Gan, J. J. Krajewski, and C. B. Eom, Integr. Ferroelectr. **21**, 499 (1998).
[6]J.-P. Maria, W. Hackenberger, and S. Trolier-McKinstry, J. Appl. Phys. **84**, 5147 (1998).
[7]S. Stemmer, G. R. Bai, N. D. Browning, and S. K. Streiffer, J. Appl. Phys. **87**, 3526 (2000).
[8]G. R. Bai, S. K. Streiffer, P. K. Baumann, S. Stemmer, O. Auciello, K. Ghosh, A. Munkholm, C. Thompson, R. A. Rao, and C. B. Eom, Appl. Phys. Lett. **76**, 3106 (2000).
[9]M. Boota, E. P. Houwman, M. D. Nguyen, G. Lanzara, and G. Rijnders, AIP Adv. **6**, 055303 (2016).
[10]P. Chekhonin, M. Mietschke, D. Pohl, F. Schmidt, S. Fähler, W. Skrotzki, K. Nielsch, and R. Hühn, Mater. Charact. **129**, 234 (2017).
[11]U. Gabor, D. Vengust, Z. Samardžija, A. Matavž, V. Bobnar, D. Suvorov, and M. Spreitzer, Appl. Surf. Sci. **513**, 145787 (2020).
[12]M. Boota, E. P. Houwman, M. Dekkers, M. Nguyen, and G. Rijnders, Appl. Phys. Lett. **104**, 182909 (2014).
[13]S. T. Hong and T. Wu, Mater. Lett. **23**, 221 (1995).
[14]T. Nakamura, A. Masuda, A. Morimoto, and T. Shimizu, Jpn. J. Appl. Phys. **35**, 4750 (1996).
[15]M. C. Jiang, T. Hong, and T. B. Wu, Jpn. J. Appl. Phys. **33**, 6301 (1994).
[16]Y. Takeshima, K. Shiratsuyu, H. Takagi, and K. Tomono, Jpn. J. Appl. Phys. **34**, 5083 (1995).
[17]M. C. Jiang and T. B. Wu, J. Mater. Res. **9**, 1879 (1994).
[18]D. H. A. Blank, M. Dekkers, and G. Rijnders, J. Phys. D: Appl. Phys. **47**, 034006 (2014).
[19]M. Boota, E. P. Houwman, G. Lanzara, and G. Rijnders, J. Appl. Phys. **128**, 055302 (2020).
[20]G. Koster, B. L. Kropman, G. J. H. M. Rijnders *et al.*, Appl. Phys. Lett. **73**, 2920 (1998).
[21]G. Rijnders, D. H. A. Blank, J. Choi, and C. B. Eom, Appl. Phys. Lett. **84**, 505 (2004).
[22]R. G. Polcawich and S. T. McKinstry, J. Mater. Res. **15**, 2505 (2000).
[23]R. G. Polcawich *et al.*, IEEE Trans. Microw. Theory Tech. **55**, 2642 (2007).
[24]A. K. Tagantsev and G. Gerra, J. Appl. Phys. **100**, 051607 (2006).
[25]V. Nagarajan, C. S. Ganpule, B. Nagaraj, S. Aggarwal, S. P. Alpay, and A. L. Roytburd, Appl. Phys. Lett. **75**, 4183 (1999).
[26]S. Gariglio, N. Stuki, J. M. Triscone, and G. Triscone, Appl. Phys. Lett. **90**, 202905 (2007).